Langmuir

Article

pubs.acs.org/Langmuir

Inner Structure of Adsorbed Ionic Microgel Particles

Stefan Wellert,*[,‡] Yvonne Hertle,[§] Marcel Richter,[‡] Martin Medebach,[‡] David Magerl,[∥] Weinan Wang,[∥] Bruno Demé,[⊥] Aurel Radulescu,[#] Peter Müller-Buschbaum,[∥] Thomas Hellweg,[§] and Regine von Klitzing[‡]

[‡]Stranski Laboratorium für Physikalische und Theoretische Chemie, Technische Universität Berlin, Straße des 17 Juni 124, 10623 Berlin, Germany

[§]Physikalische und Biophysikalische Chemie (PC III), Universität Bielefeld, Universitätsstraße 25, 33615 Bielefeld, Germany

[∥]Physik-Department, Lehrstuhl für Funktionelle Materialien, Technische Universität München, James-Franck-Straße 1, 85748 Garching, Germany

[⊥]Institut Laue Langevin, 6 Rue Jules Horowitz, 38042 Grenoble, France

[#]Heinz Maier Leibnitz Zentrum, Lichtenbergstraße 1, 85747 Garching, Germany

ABSTRACT: Microgel particles of cross-linked poly(NIPAM-*co*-acrylic acid) with different acrylic acid contents are investigated in solution and in the adsorbed state. As a substrate, silicon with a poly(allylamine hydrochloride) (PAH) coating is used. The temperature dependence of the deswelling of the microgel particles was probed with atomic force microscopy (AFM). The inner structure of the adsorbed microgel particles was detected with grazing incidence small angle neutron scattering (GISANS). Small angle neutron scattering (SANS) on corresponding microgel suspensions was performed for comparison. Whereas the correlation length of the polymer network shows a divergence in the bulk samples, in the adsorbed microgel particles it remains unchanged over the entire temperature range. In addition, GISANS indicates changes in the particles along the surface normal. This suggests that the presence of a solid surface suppresses the divergence of internal fluctuations in the adsorbed microgels close to the volume phase transition.

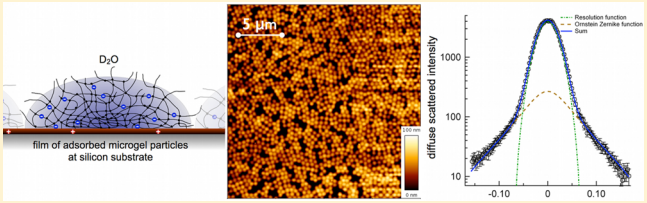

INTRODUCTION

Due to the tunability of their softness and fast response to various external stimuli (temperature, pH, and ionic strength), colloidal suspensions of microgel particles are studied with aiming at an understanding their basic physical properties.[1−6] Among these systems poly(*N*-isopropylacrylamide) (PNIPAM) is the most intensively explored. As a result of numerous experimental and theoretical investigations, the swelling/deswelling behavior of uncharged homopolymer microgels and gels is well understood. From a theoretical point of view the Flory−Rehner theory is successful in explaining the swelling/deswelling behavior as an interplay of osmotic pressure contributions.[7] A variety of experimental methods such as static and dynamic light scattering, elastic and quasielastic small-angle neutron scattering,[8−11] NMR,[12] and imaging techniques are used for the characterization of the microgel bulk phase morphology, the internal network structure, the dynamics, and the swelling/deswelling behavior. For ionic microgel particles, formed by the incorporation of ionizable comonomers into the gel network, the situation becomes more complex.[13−17] Experimentally, many similarities among ionic microgels, polyelectrolytes, and biopolymer gels were found.[18−20] Introducing charges into the network adds a tunable electrostatic contribution to the effective interaction between pairs of microgel particles. Moreover, loosely cross-linked ionic microgels combine properties of hard spheres and soft particles, and the soft repulsive interaction was investigated theoretically and experimentally.[21−23] However, theoretical concepts for nonionic microgels cannot be easily applied and extended to these charged systems. A prediction of the swelling/deswelling behavior requires an extension of the total osmotic pressure by additional terms describing fixed charge−charge repulsion, counterion condensation, and the Donnan potential accounting for coion effects and background electrolytes.[22] Recent studies investigated the specific features of the swelling behavior of ionic microgels.[24−26]

With respect to adsorbed microgel films, even less is known since these systems have only been rarely investigated. AFM and ellipsometry measurements demonstrated the conservation of the stimuli-responsivity in the adsorbed state and the possibility of preparing densely packed layers.[27−31] Coatings based on these particles are envisioned as new actuators, controlled release systems, smart cell culture substrates,[32] biosensors, and thermomechanical devices.[33,34] Dense packing, interparticle interaction, overlapping of dangling ends of neighboring particles, particle compression, and the interactions between the surface and the particles prevent a simple application of the bulk phase behavior concepts to the adsorbed state. It has been shown that poly(NIPAM-*co*-acrylic acid) microgel particles in bulk solution exhibit a two-step

Received: February 5, 2014
Revised: May 27, 2014
Published: June 12, 2014

   dx.doi.org/10.1021/la500390j | *Langmuir* 2014, 30, 7168−7176

phase transition (at 32 and 45 °C),[35] at least for higher comonomer contents. Other studies report a single-step transition.[16,36] However, particles adsorbed on a gold surface exhibit only one VPT.[37] Most studies in the adsorbed state analyzed single, well-isolated particles to exclude effects due to dense packing. Beside the temperature-dependent morphology of the particle layers, their internal structural properties are also of interest. However, these are not directly accessible by techniques such as AFM and ellipsometry.[38,39] The swelling behavior of adsorbed particles could only be modeled using only a modified Flory–Rehner approach.[27] The application of neutron scattering techniques provides direct access to these internal properties. Small-angle neutron scattering (SANS) gives access to the relevant length-scale regime.[40−43]

Because the sample volume of a monolayer of microgel particles on a substrate is much smaller as compared to that of typical bulk samples probed with SANS, simple SANS measurements cannot be performed. Grazing incidence small-angle neutron scattering (GISANS) is a powerful technique for overcoming this problem.[44] GISANS was used successfully for the investigation of polymer droplets on solid supports which resemble a similar scattering volume to that of the microgel particles.[45,46] Due to the presence of water surrounding the microgel particles and thus the need to use a liquid cell, the GISANS experiment becomes more complex. In the present work, the aim is the detection of a small length scale on the order of a few nanometers, which will have its related GISANS signal at rather high values of the scattering vector. This makes the scattering experiment reported in this work a challenging task. The experimental situation is sketched in Figure 1. To

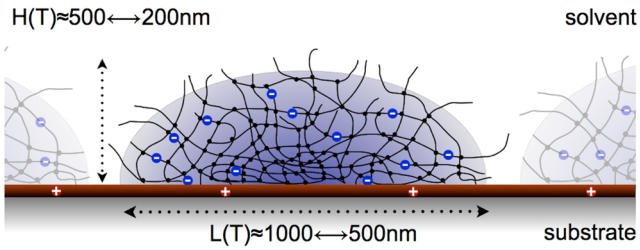

Figure 1. Schematic representation of the sample. Adhesive charged poly(NIPAM-*co*-acrylic acid) microgel particles are organized in a monolayer at an oppositely charged surface. Typically, silicon surfaces coated with a polyelectrolyte layer serve as an adherend. Beside van der Waals forces, repulsive and electrostatic interactions contribute to the adhesive–adherent interaction.

provide sufficient scattering signal, a densely packed monolayer of gel particles, swollen with solvent (water) with a height of a few hundred nanometers, is in contact with a solvent reservoir (height 10^3 to 10^4 times larger than the particle layer). The contact with the solid charged surface introduces a particle compression. The attractive interaction between surface and particles leads to the spherical cap-type shape of the particles. In contrast to studies on isolated particles, dense packing results in interparticle interaction and the overlapping of dangling ends of neighboring particles. The present paper combines AFM and GISANS measurements and focuses on the temperature dependence of the fluidlike thermal network fluctuations in adsorbed microgel particles. Due to the large solvent reservoir above the adsorbed layer, no osmotic deswelling is expected due to high counterion concentrations in the solvent and due to the lateral packing of the adsorbed particles. AFM measurements in a temperature-controlled liquid cell were used to determine the swelling/deswelling of the microgel particles on the surface during the temperature-induced volume phase transition. In addition, SANS and DLS measurements on microgels in suspension were done for reference and compared to results from GISANS experiments.

EXPERIMENTAL SECTION

Microgel Preparation. Two ionic microgel systems of different comonomer concentrations were synthesized. Monomer (*N*-isopropylacrylamide, NIPAM, Aldrich, 97%), cross-linker (*N*,*N*-methylenebisacrylamide, BIS, Aldrich, 99.5%), comonomer (acrylic acid, AAc, Aldrich, 99%), and radical starter (potassium persulfate, KPS, Fluka, 99%) were used as received. The microgels were synthesized using a cross-linker content of 2 mol % BIS (related to the amount of NIPAM) and comonomer contents of 5 and 20 mol % AAc in relation to the total monomer content including the cross-linker. The microgel synthesis was performed via precipitation polymerization without additional surfactant as described elsewhere.[47] Both systems are named according to the nominal comonomer content, microgels AAc-5 and AAc-20. Titration was performed to determine the effective AAc amount incorporated into the microgels. A 0.5 wt % microgel solution was titrated with 2.5 mM NaOH in a Titrando 836 (Metrohm GmbH, Germany).[37] The effective AAc contents for samples AAc-5 and AAc-20 were 2.2 and 18.2 mol % AAc.

For the AFM and GISANS measurements the microgels were spin-coated onto poly(allylamine hydrochloride) (PAH)-covered silicon wafers. This initial layer of the weakly charged polyelectrolyte was used to support the adhesion of microgel particles via electrostatic interaction between the positively charged surface and the negatively charged microgel particles. Spin coating was done using a P6700 spin coater (SCS, Inc., Indianapolis, IN, USA). All preparations were carried out at room temperature in a clean room environment by applying 2000 rpm for 300 s at an initial concentration of 0.05 wt %. Under these conditions adsorbed films of well-separated microgel particles were obtained on silicon wafer surfaces of 2 × 2 cm^2. For GISANS experiments 500 rpm for 300 s with an initial concentration of 1 wt % were chosen as the spin-coating conditions to prepare a close-packed monolayer on a 5 × 8 cm^2 surface of a silicon single-crystal block (Siliciumbearbeitung Holm, Germany).

Deuterated water of 99.90% isotopic purity (Eurisotop, France) was used as a solvent.

For all measurements in water, a three-stage Millipore Milli-Q Plus 185 was used for purification. The pH values for all used solutions were pH 5.8 for AAc-5 and pH 5.5 for AAc-20. No salt was added to tune the pH. In the case of D_2O, no further pD adjustment was made. Consequently, in all measurements the microgel samples were largely ionized to provide strong adhesion to the solid surface. For comparison of the bulk behavior, samples of AAc-5 and AAc-20 were also measured at pH 2. In this case the pH was tuned by the addition of HCl.

AFM Measurements. All AFM measurements were performed with a JPK NanoWizard II (JPK Instruments, Berlin, Germany). The particle imaging was done using a thermostatted liquid cell. Uncoated CSC37 silicon cantilevers were obtained from Micromasch (Wetzlar, Germany). The sample temperature was varied from 20 to 60 °C to follow the thermoresponsivity and to determine the VPT temperature. Calculation of the particle volume in the adsorbed state was done according to the literature.[37] The measured cross section is rotated around the *y* axis with the assumption of rotational symmetry. The volume created by that rotation was calculated numerically, according to eq 1

$$V = \pi \int_0^H f^2(h)\, \mathrm{d}h \tag{1}$$

where H is the height of the adsorbed microgel, $f(h)$ is the cross-sectional profile, and h is the slow-scan axis. The volume of the adsorbed particles was determined from independent measurements of at least three particles.

dx.doi.org/10.1021/la500390j | *Langmuir* 2014, 30, 7168−7176

Dynamic Light Scattering Measurements. Dynamic light scattering (DLS) measurements were performed using an ALV goniometer setup equipped with an Nd/YAG laser operated at a wavelength of 532 nm. The swelling/deswelling behavior was measured in the temperature range between 20 and 60 °C with a microgel dispersion concentration of 0.01 wt %. Intensity−time autocorrelation functions were recorded at a fixed scattering angle of 60°. The data were analyzed by inverse Laplace transformation applying the CONTIN algorithm. Data obtained at 20 and 50 °C in the protonated and deprotonated states were used for the comparison of the particle volumes in the bulk and adsorbed on the silicon surface.

SANS Measurements. *Experimental Details.* SANS measurements were made on the KWS-2 instrument of the JCNS at the FRM-II (Garching, Germany). At a neutron wavelength of 5 Å, three sample-to-detector distances (2.05, 8, and 20 m) were combined to cover a Q range from 0.001 to 0.4 $Å^{-1}$. The neutron beam collimation was adapted to sample−detector distances of 2.05, 8, and 20 m. A sample of the AAc-5 microgel system was measured in quartz cells with a 2 mm neutron path way. Measurements were made at eight temperatures in the range from 20 to 55 °C. The sample was thermostatted at the desired temperature using a thermocycle with a stability of ±0.1 K and equilibrated at each temperature for 15 min prior to the SANS measurement.

Data Analysis. Raw scattering data were initially treated, radially averaged, and brought to absolute scale by the procedures provided by JCNS using the QtiKWS10 software. Figure 2 shows example of two representative SANS curves measured for sample AAc-5 at temperatures of 20 and 55 °C. Due to the large size of the microgel particles and the selected resolution in the SANS experiment, form factor oscillations do not lie within the experimental Q range. Thus all SANS data are fitted with eq 2.

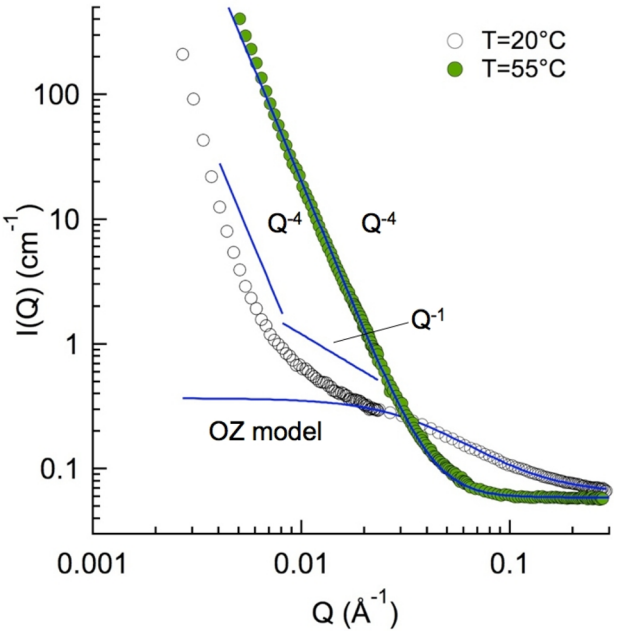

Figure 2. Examples of SANS data measured for sample AAc-5 at 20 and 55 °C. The curve measured at 20 °C contains contributions from the Porod regime and the Ornstein−Zernike part. In between both contributions, the intensity is proportional to Q^{-1}. At 55 °C, the Porod regime dominates the signal.

To analyze the SANS data, a model using a superposition of the Ornstein−Zernike scattering function, the Porod law, and an internal incoherent sample background was selected. This model has been frequently used to fit SANS data of neutral microgels and corresponds to a scattering contribution from the particle surface and the scattering from solvated fluctuating polymer chains.[48] For weakly charged ionic gels the same model is assumed to be applicable.[49] Other authors applied a modified squared Lorentz function based on the Debye−Bueche function in combination with the sum of a power law and an Ornstein−Zernike contribution to describe their data.[50] This treatment is different compared to the analysis of small-angle scattering data from macrogels. In macrogels, no Porod scattering occurs. Instead, one observes a Guinier-like decay related to the distance between the chemical cross-links. In microgels, this length scale related to the chemically fixed network cannot be resolved. Only the dynamic solutionlike correlation length is observed. In the case of pure polyelectrolyte gels, the observation of a second length scale due to the locally stretched polymers was reported.[18] Moreover, for neutral PNIPAM microgels it was reported that two distinct length scales related to chain dynamics can be resolved, one stemming from the dense core and the other one from the loosely cross-linked shell.[40] However, for the analysis of the scattering curves of sample AAc-5 we used the combination of the Porod scattering law and the Ornstein−Zernike equation given by

$$I(Q) \propto \Delta\rho \frac{A}{V}\frac{1}{Q^{\alpha}} + \frac{I_L(0)}{1+\xi^2 Q^2} \tag{2}$$

A/V denotes the surface area per unit volume, and $\Delta\rho$ is the contrast in terms of the difference in scattering length densities of the microgel particles and the surrounding solvent. The exponent is $\alpha = 4$ in the ideal case of smooth surfaces according to the predictions of the Porod scattering law. The liquidlike correlations in the polymer network decay with the dynamic correlation length ξ. ξ is approximately a factor of 5−10 smaller compared to the mean distance between the chemical cross-links.

GISANS Measurements. *Experimental Details.* GISANS measurements were performed at the D16 instrument at the ILL (Grenoble, France). A sample−detector distance of 1 m was used to access a large Q range. An evacuated neutron flight path and a vertically focused monochromatic neutron beam (wavelength of 4.76 Å) were selected. The neutron beam was focused onto the detector to make use of the 120 mm beam height of the primary beam and thus achieve high-flux conditions. The focal spot on the detector was 17 mm in the vertical direction and an additional guard slit was mounted in front of the sample to optimize the background conditions. The samples were mounted in a custom-made D_2O-filled liquid cell to enable the investigation of the solid−liquid interface. In this cell, the sample surface is sealed against air by using a Teflon trough inside an aluminum housing. Thermal equilibration and temperature control inside the sample cell were achieved by cooling water circulation through the aluminum housing. A Pt100 element was placed inside the trough close to the sample surface. The neutron beam entered the sample through the silicon block. In order to reduce the background, additional Cd shielding at the entrance and exit sides were used to block the direct neutron beam and parasitic scattering.

In Figure 3 the GISANS geometry is depicted. The sample surface is oriented in the $x - y$ plane, and the neutron beam enters and leaves the surface with an initial angle α_i and a scattering angle α_f in the scattering plane defined by the x and z planes. In the case of diffuse scattering due to lateral structures in the sample, contributions out of this scattering plane at an additional lateral scattering angle of $2\theta_f$ occur. In GISANS geometry, the components of the scattering vector Q are defined by

$$Q_x = \frac{2\pi}{\lambda}(\cos 2\theta_f \cos \alpha_f - \cos \alpha_i) \tag{3}$$

$$Q_y = \frac{2\pi}{\lambda}(\sin 2\theta_f \cos \alpha_f) \tag{4}$$

$$Q_z = \frac{2\pi}{\lambda}(\sin \alpha_i + \sin \alpha_f) \tag{5}$$

and probed depending on the chosen type of scattering experiment. The critical angle of total reflection α_c is given by

dx.doi.org/10.1021/la500390j | Langmuir 2014, 30, 7168−7176

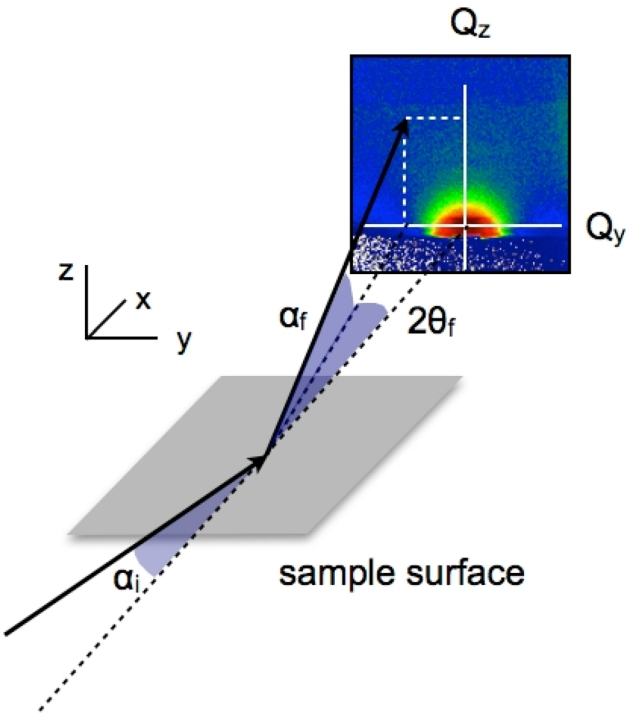

Figure 3. Scheme of a GISANS experiment. Vertical cuts along the Q_z direction and horizontal cuts along the Q_y direction are indicated.

$$\alpha_c = \lambda\sqrt{\frac{Nb}{\pi}} \tag{6}$$

Here, λ is the neutron wavelength, N is the atomic number density, and b is the bound coherent scattering length. From the experimental conditions, $\alpha_c = 0.3°$ was calculated by taking into account the scattering length densities of $\rho = 6.35 \times 10^{-6}$Å^{-2} for D_2O and $\rho = 5.84 \times 10^{-6}$Å^{-2} for the microgel. The scattering depth D of the neutrons determines the experimentally accessible volume in the near surface region of the sample and is given by

$$D = \frac{\lambda}{\sqrt{2}\pi(l_i + l_f)} \tag{7}$$

where $l_{i,f}$ depend on the critical angle of incidence α_c and the angles of the incident beam α_i and reflected beam α_f.[44,51]

$$l_{i,f} = \left((\alpha_c^2 - \alpha_{i,f}^2) + \sqrt{(\alpha_{i,f}^2 - \alpha_c^2)^2 + 4\beta^2}\right)^{1/2} \tag{8}$$

Within the distorted wave Born approximation (DWBA), the differential cross section is separable in a specular signal and a perturbed diffuse scattering contribution

$$I_{surf}(Q) = I_{spec}(Q) + I_{diff}(Q) \tag{9}$$

Within the effective surface approximation, the diffuse scattering part can be simplified to[52]

$$I_{diff}(Q) \propto S_{DBWA}(Q) = S_{BA}(Q)\, T_i^2(\alpha_i)\, T_f^2(\alpha_f) \tag{10}$$

where A is the illuminated surface area, $T_{i,f}$ represents the Fresnel transmission functions for incident and reflected beams, and $S(Q)$ is the diffuse-scattering factor. The Fresnel transmission functions act only as overall scaling factors in the GISANS geometry because $\alpha_{i,f}$ are fixed.

Data Analysis. Initial data treatment was done using the LAMP software provided by the ILL. Selected line cuts of the two-dimensional (2D) GISANS data were done. A vertical line cut at $Q_y = 0$ along the Q_z direction and a horizontal line cut at constant Q_z at the position of the Yoneda peak along the Q_y direction were selected for analysis.

Figure 4 depicts examples of the background-corrected GISANS data from an adsorbed ionic microgel film. In graph a, vertical line cuts

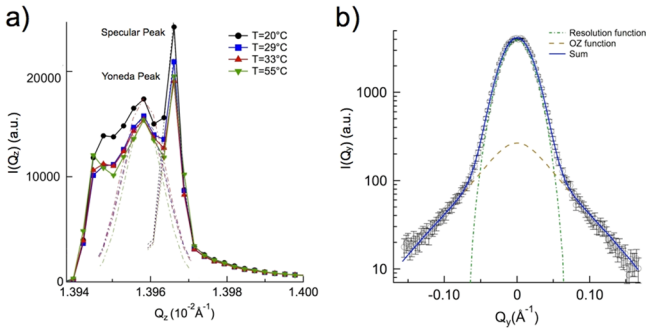

Figure 4. (a) Examples of the background-corrected GISANS data from an adsorbed ionic microgel film. Vertical line cuts at four temperatures below, above, and close to the VPT. The dashed and dashed−dotted lines are fits of a Gaussian profile to the Yoneda and the specular peaks. (b) Horizontal line cut at 20 °C. The model for the quantitative description consists of the sum (solid line) of a Gaussian function approximating the instrumental resolution function (dashed−dotted line) and a Lorentzian curve describing the lateral Ornstein−Zernike contribution in the wings of the Yoneda peak (dashed line). The sum of both components is shown as a solid line.

at four temperatures below, above, and close to the VPT are shown. The dashed and dashed−dotted lines are fits of a Gaussian profile to the Yoneda and the specular peak. Graph b shows a horizontal line cut at 20 °C. The model for the quantitative description

$$F(Q) = A\exp\left(-\frac{(Q - Q_{max})^2}{2\sigma^2}\right) + \frac{I_L(0)}{1 + \xi^2 Q^2} \tag{11}$$

consists of the sum (solid line) of a Gaussian function approximating the instrumental resolution function (dashed−dotted line) and a Lorentzian curve describing the lateral Ornstein−Zernike contribution in the wings of the Yoneda peak (dashed line). The sum of both components is shown as a solid line.

RESULTS AND DISCUSSION

Deswelling of a Monolayer of Microgel Particles. In real space the sample surface is imaged with AFM. Figure 5a shows four AFM micrographs of temperature-dependent height profile measurements in a thermostatted liquid cell on single adsorbed microgel particles for systems AAc-5 and AAc-20 at 20 and 50 °C. At 20 °C the particle size is larger than at 50 °C in both systems. This confirms that temperature-dependent deswelling is still possible in the adsorbed state for both systems. In Figure 5b the densely packed adsorbed microgel particles (AAc-5) in the dry state are shown. The measurement was done after the GISANS experiment and illustrates the stability of the adsorbed layer even over the long measurement time of the GISANS experiment.

In Figure 6 the swelling ratio $\alpha(T)$ (volume normalized with respect to particle volume at 20 °C and values calculated using eq 1) for AAc-5 and AAc-20 is shown. The swelling ratio decreases from $\alpha = 1$ at 20 °C to $\alpha = 0.4$ for AAc-5 and $\alpha = 0.2$ for AAc-20 in the deswollen state at 50 °C. The volume phase transition temperatures are 43 °C for AAc-5 and 45 °C for AAc-20. The shift of the VPTT compared to the VPTT in the bulk results from the electrostatic repulsion and the osmotic pressure inside the charged polymer network.[37] The electro-

dx.doi.org/10.1021/la500390j | Langmuir 2014, 30, 7168−7176

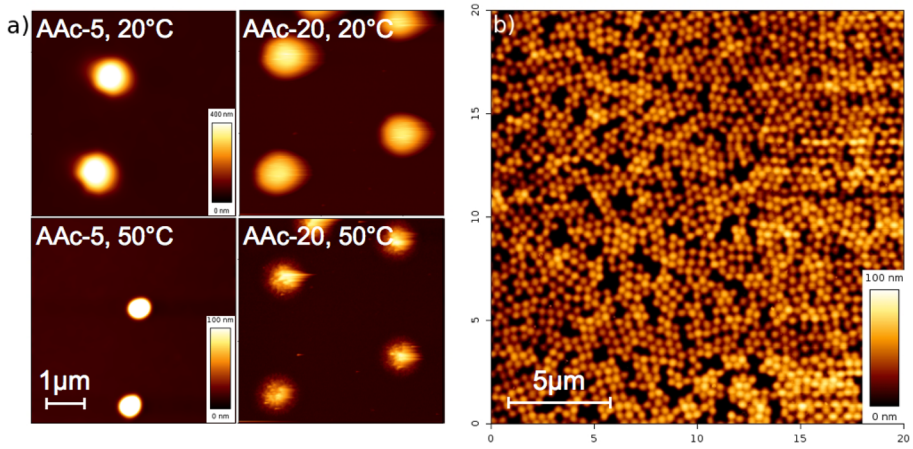

Figure 5. (a) AFM images of AAc-5 in water taken in intermittent contact mode at 20 and 50 °C, respectively. The scan size is 5 × 5 μm^2. (b) Densely packed adsorbed microgel particles (AAc-5) in the dry state measured after the GISANS experiment. Here, the scan size is 20 × 20 μm^2.

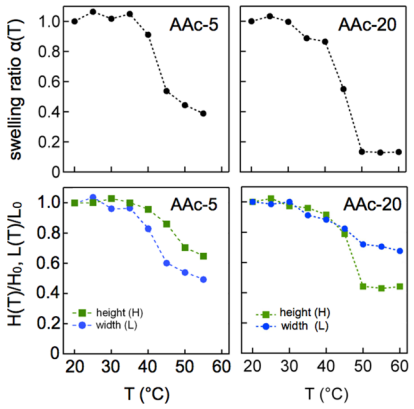

Figure 6. Top row: Volume ratio vs temperature for AAc-5 (left) and AAc-20 (right). Bottom row: Microgel height and microgel width vs temperature for AAc-5 (left) and AAc-20 (right). The particle height $H(T)$, width $L(T)$, and volume were extracted from the particle cross sections. The data are normalized to values at 20 °C.

static repulsion expands the polymer chains and thereby the network. Intimately linked with this is the increase in the osmotic pressure due to the increase in the counterion concentration inside the microgel particles.[24,25] The temperature dependences of particle height $H(T)$ vertical to the surface and the lateral particle dimension $L(T)$ parallel to the surface were extracted from the cross sections of the AFM height profiles, normalized ($H_0 = H(T_0)$ and $L_0 = L(T_0)$, T_0 = 20 °C) and plotted as a function of temperature, as shown in Figure 6.

Table 1 summarizes the results of DLS and AFM measurements in terms of particle volumes in the suspension and the adsorbed state. The particle volumes in the swollen and deswollen states in the bulk were calculated from hydrodynamic radii R_h measured for both systems at 20 and 50 °C. For comparison the hydrodynamic radii of both samples at pH 2 at both temperatures are added to the table. In the charged state the size is larger than at pH 2, where the chargeable groups are protonated. The particle volumes at the solid surface are much smaller with respect to the bulk values. However, the relative differences between the values of AAc-5 and AAc-20 remain very similar in the adsorbed state compared to the bulk data. Beside the large difference in volume in relation to the bulk values, this leads to a stronger deswelling effect for AAc-20. It was observed that an increasing content of acrylic acid has the same effect on the microgel elasticity as the reduction of the cross-linker content.[53,54]

Inner Structure of Microgel Particles in Solution. It is well known that thermoresponsive bulk gels and microgels in solution exhibit an increase in ξ when approaching VPTT. Therefore, here we present only the temperature-dependent data of AAc-5 to underline this exemplary behavior in the present study. To probe the temperature-responsive behavior of the microgel particles, SANS measurements for eight different temperatures between 20 and 55 °C were performed. The SANS data were fitted using a superposition of the Ornstein–Zernike scattering function, the Porod law, and an internal incoherent sample background (eq 2). The resulting correlation length ξ is shown as a function of temperature in Figure 7. In the swollen state at 20 °C, a value of ξ = 25 Å was found for AAc-5. (For AAc-20 at 20 °C a value of 28 Å was obtained from SANS measurements not shown here.) Increasing the sample temperature changes the solvent condition, and ξ strongly increases up to its maximum value of 90–100 Å in the temperature range of 34–36 °C. A further temperature increase reduces ξ again as the VPT is passed. At a temperature of 45 °C the data indicate a second and less pronounced decrease in ξ from 30 to 10 Å. In the intermediate Q range of the SANS data

Table 1. Summary of the Hydrodynamic Radii of AAc-5 and AAc-20 in Suspension[a]

	R_h (nm)[b]		R_h (nm)[c]		V_{bulk} (10^7 nm^3)		V_{ads} (10^7 nm^3)			
	20 °C	50 °C	20 °C	50 °C	20 °C	50 °C	20 °C	50 °C	H_0 (nm)	L_0(nm)
AAc-5	470	93	563	323	75	14	9.6	3.4	363	1000
AAc-20	590	80	980	275	394	9	12	1.5	270	1133

[a]Particle volumes in suspension (deprotonated state) and in the adsorbed state at 20 and 50 °C and the values of H_0 and L_0 at 20 °C. [b]At pH 2. [c]At pH 5.8 and 5.5.

dx.doi.org/10.1021/la500390j | Langmuir 2014, 30, 7168–7176

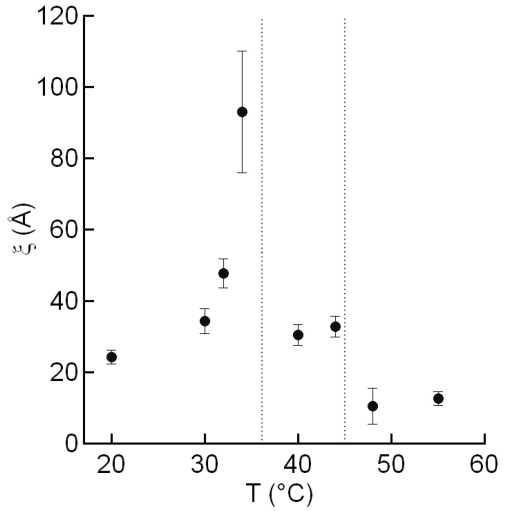

Figure 7. Correlation length ξ of sample AAc-5 in the temperature range between 20 and 55 °C in solution (SANS). At the VPT, ξ diverges and decreases strongly at temperatures above that point. VPT and the second transition are marked with dashed lines.

at temperatures below the VPT the scattering intensity is proportional to Q^{-1}. Such a region was also reported for polyelectrolyte gels and suggests the presence of an additional length scale in the network due to locally stretched polymers or structural heterogeneities.[18]

Inner Structure of the Microgel Particles on a Solid Support. With GISANS, the network correlation length of the microgel particles on the solid support is determined. The GISANS geometry is sketched in Figure 3. The 2D GISANS data were analyzed in vertical and horizontal line cuts as shown in Figure 4. Figure 8 compares exemplarily horizontal line cuts of the 2D GISANS data measured for an adsorbed microgel film immersed in D_2O for three sample temperatures at the position of the Yoneda peak. The temperatures are chosen below, close to and above the VPT. The solid lines are fits using eq 11. At low Q_y values the resolution function determines the

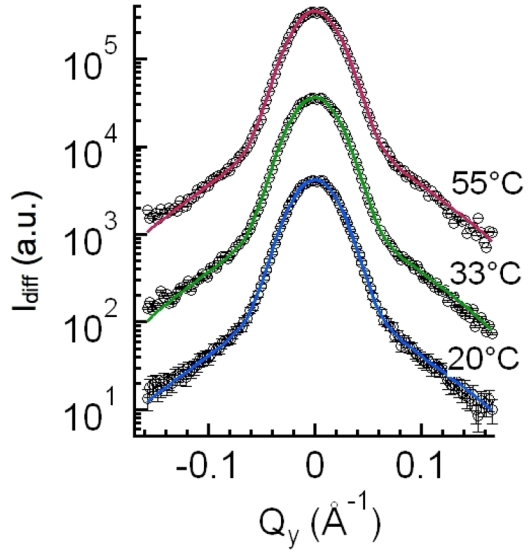

Figure 8. Horizontal line cuts of the 2D GISANS data (circles) measured for sample AAc-5 at three sample temperatures. The solid lines show the corresponding fits.

diffuse intensity distribution $I_{diff}(Q_y)$. This contribution is well approximated by a Gaussian function. The diffuse scattering from the sample dominates the scattering intensity at values $Q_y > 0.05$ Å^{-1}. In this Q_y range, the intensity is fitted with an Ornstein–Zernike-type function according to the bulk-phase scattering properties. The model fits the scattering intensity over the whole measured Q_y range. Within the experimental error the scattering intensity at high Q_y values shows no differences at the three temperatures. Only the shoulder in the intermediate Q range from 0.02 to 0.1 Å^{-1} is not observed in the GISANS data at temperatures below the volume phase transition. This experimental observation indicates a reduced contribution of the thermal density fluctuations to the scattering intensity.

The vertical cuts were used to analyze the intensity of the specular peak. Figure 9a compares the peak intensities of the

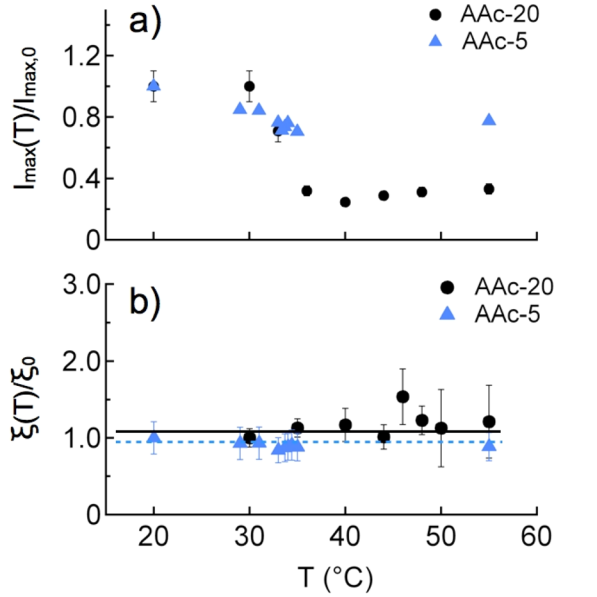

Figure 9. (a) Normalized intensity of the specular peak for samples AAc-5 and AAc-20 shown as a function of temperature. (b) Temperature dependence of the correlation lengths ξ for samples AAc-5 and AAc-20. $\xi(T)$ is normalized to $\xi(T_0)$, where T_0 is the lowest temperature in each measurement series to allow for a comparison between both samples. Solid and dashed lines are guides to the eye.

specular peak in the investigated temperature range for both samples. For better comparability, all intensities are normalized to the corresponding intensities at T = 20 °C. The peak intensity decreases for both samples, and for sample AAc-20 the trend is more pronounced, which is related to the stronger shrinking effect, already demonstrated in Figure 6. The temperature dependence of the maximum intensity of the Yoneda peak is not shown. It remains nearly constant in the case of sample AAc-5 and increases only very slightly for sample AAc-20 with increasing temperature. The temperature dependence of the specular peak intensity corresponds to the behavior observed in the AFM measurements on isolated particles of type AAc-5 and AAc-20 as described above. The deswelling of the particles with increasing temperature changes the scattering length density of the layer in the GISANS experiment due to the increasing expulsion of the deuterated water. As a result, the critical angle and the position of the edge of external total

dx.doi.org/10.1021/la500390j | Langmuir 2014, 30, 7168−7176

reflection for the neutrons change. Thus the specular intensity is affected. The less pronounced changes in the Yoneda peak intensities reflect the absence of a serious lateral roughening of the films. Therefore, the temperature dependence of the specular and Yoneda peak intensities indicate structural changes in the densely packed adsorbed microgel film in the direction along the surface normal only.

To extract structural information related to the hydrogel network, the correlation length $\xi(T)$ for both samples is determined. Figure 9b shows these values normalized to the value at the lowest measured temperature ($\xi_0(T_0)$, $T_0 = 20$ °C). The absolute values of ξ are 21 Å for AAc-5 and 18 Å for AAc-20 at T_0. Within the precision of the experiment, no significant changes in the correlation length are visible upon crossing the VPT. This finding is contrary to the behavior in solution which was probed with the SANS measurements. Both the absence of a pronounced shoulder in the intensity in the intermediate Q_y range and the temperature dependence of $\xi(T)$ indicate a significant confinement effect on the volume phase transition of the adsorbed microgel particles. Most likely this confinement is introduced by the solid substrate. Effects due to interaction with neighboring microgels cannot be completely ruled out at the high 2D packing densities in the layers studied here. However, the temperature-dependent AFM measurements in the present and also in previous works show that the particles swell only marginally in plane. Therefore, we think that confinement due to a high packing density has only a small or no influence on the fluctuations of the correlation lengths in the present case. The cross-linked polymer network deswells, but this seems not to influence the fluidlike thermal fluctuations of the network. Modifications of the behavior of critical fluctuations in a confined state with respect to the bulk are also known for binary fluid mixtures.[55,56] Moreover, confinement effects due to the presence of a solid impenetrable wall are also discussed to be of importance for structure and wall−polymer interactions in the case of polyelectrolyte stars close to a wall.[57] In general, our experimental observations would correspond to a stiffening of the polymer network. This interpretation is in line with the recent observation that the divergence of ξ is also suppressed in solution if the microgels have a cross-linker content of 15 mol % or more.[58] Possible reasons for the stiffening of the adsorbed state are electrostatic interactions between network and surface and deformation and compression of the polymer network inside the hemispherically shaped adsorbed microgel particles. The electrostatic attraction has been proven by the addition of salt. Due to screening, the particles start to swell.[38,59] Speculatively, such effects inside the adsorbed particles should be pronounced in the vicinity of the solid surface. With increasing vertical distance z from the surface, the polymer network properties inside the adsorbed particles should become similar to those of a freely diffusing microgel particle of the same composition and temperature. Ionic microgel particles exhibit soft repulsive interactions. Due to the close packing and possible interpenetration of the dangling polymer chains of the particles in the region close to the solid surface, additional repulsive interactions could be introduced into the system, which then contribute to the observed stiffening.

It should be noted that the GISANS measurements were performed with $\alpha_i > \alpha_c$, which gives rise to a very large scattering depth of the neutrons. As a consequence, the diffuse intensity was collected from the entire height of the adsorbed particle layer. Close to the solid surface the polymer concentration is larger than in the loosely connected outer shell region of the microgel particles. Scattered neutrons from near the surface might contribute more strongly to the GISANS signal than would neutrons scattered from the shell region. In addition, AFM measurements[39] suggest an interaction of the polymer chains with the substrate, which leads to a partial collapse due to the adsorption process. As a result, an enhanced stiffness of the network gives an enhanced bulk modulus. A stiffening of the network would reduce the amplitude of thermal fluctuations and suppress the corresponding scattering signal.

Our combined SANS, AFM, and GISANS experiments show that microgel particles behave significantly differently on the local scale if dissolved in solution or positioned on a solid and charged support.

CONCLUSIONS

The temperature dependences of the correlation length of network fluctuations in weakly negatively charged poly(NIPAM-co-AAc) microgel particles adsorbed onto positively charged silicon substrate surfaces and in bulk solution are compared. The macroscopically observable volume phase transition in the adsorbed state is well detectable in AFM measurements and by the change in the specular intensity in the GISANS measurements. The deswelling of the AAc-20 microgel particles is more pronounced as compared to that of AAc-5 microgel particles due to a more fluffy structure. In solution, the temperature dependence of the correlation length ξ is probed with SANS measurements. For an ionic microgel with an effective AAc content of 2.2 mol %, a behavior similar to that of pure homopolymer PNIPAM microgels is found. The analysis of the temperature-dependent GISANS measurements shows a decrease in the specular peak intensity which corresponds to the volume phase transition in the adsorbed state and reflects changes along the surface normal. In contrast to bulk measurements, no significant contribution of the thermal density fluctuations to the scattered signal is observed, and the correlation length remains constant within the precision of the experiment. This suggests that the presence of a solid surface suppresses the divergence of internal fluctuations in adsorbed microgels. These findings reveal a significant effect of the solid substrate on the temperature dependence. This might be caused by the strong electrostatic attraction to the substrate, but also only van der Waals interactions might be sufficient to suppress the fluctuations. This remains to be investigated with microgels without AAc. In addition, the compression of the polymer network inside the hemispherically adsorbed particles could increase repulsive interactions. In general, the results of this study indicate an effective stiffening of the network in the adsorbed state and thereby underline the complexity by changing the system from volume to monolayer samples. Future surface-sensitive scattering experiments could address the influence of cross-linker and comonomer contents as well as the role of the lateral packing density of the ionic microgel particles.

AUTHOR INFORMATION

Corresponding Author

*E-mail: s.wellert@tu-berlin.de. Phone: +49 (0)30 31424958. Fax: +49 (0)30 31426602

Notes

The authors declare no competing financial interest.

■ ACKNOWLEDGMENTS

Financial support by the Deutsche Forschungsgemeinschaft in the framework of SPP 1259 "Intelligente Hydrogele" (Mu1487/8, He2995/2-3, Kl1165/7) is gratefully acknowledged. T.H. thanks the German Federal Ministry of Education and Research (BMBF) for partial support in the framework of the project "ThermoCell". We gratefully acknowledge the financial support provided by JCNS and ILL to perform the neutron scattering measurements.

■ REFERENCES

(1) Nayak, S.; Lyon, L. A. Soft Nanotechnology with Soft Nanoparticles. *Angew. Chem. Int. Ed.* **2005**, *44*, 7686−7708.
(2) Lyon, L. A.; Fernandez-Nieves, A. The Polymer/Colloid Duality of Microgel Suspensions. *Annu. Rev. Phys. Chem.* **2012**, *63*, 25−43.
(3) Ballauff, M.; Lu, Y. "Smart" nanoparticles: Preparation, characterization and applications. *Polymer* **2007**, *48*, 1815−1823.
(4) Lutz, J. F. Polymerization of Oligo(Ethylene Glycol) (Meth)-Acrylates: Toward New Generations of Smart Biocompatible Materials. *J. Polym. Sci., Part A: Polym. Chem.* **2008**, *46*, 3459−3470.
(5) Saunders, B. R.; Vincent, B. Microgel particles as model colloids: theory, properties and applications. *Adv. Colloid Interface Sci.* **1999**, *80*, 1−25.
(6) Saunders, B. R.; Laajam, N.; Daly, E.; Teow, S.; Hu, X.; Stepto, R. Microgels: From responsive polymer colloids to biomaterials. *Adv. Colloid Interface Sci.* **2009**, *147−148*, 251−262.
(7) Hirotsu, S. Static and time-dependent properties of polymer gels around the volume phase transition. *Phase Transitions* **1994**, *47*, 183−240.
(8) Wu, C.; Zhou, S. Light Scattering Study of Spherical Poly(N-isopropylacrylamide) Microgels. *J. Macromol. Sci., Part B: Phys.* **1997**, *36*, 345−355.
(9) Clara-Rahola, J.; Fernández-Nieves, A.; Sierra-Martín, B.; South, A. B.; Lyon, A. L.; Kohlbrecher, J.; Fernández-Barbero, A. Structural properties of thermoresponsive poly(N-isopropylacrylamide)-poly-(ethyleneglycol) microgels. *J. Chem. Phys.* **2012**, *136*, 214903.
(10) Shibayama, M.; Tanaka, T.; Han, C. C. Small angle neutron scattering study on poly(N-isopropyl acrylamide) gels near their volume-phase transition. *J. Chem. Phys.* **1992**, *97*, 6829−6841.
(11) Crowther, H. M.; Saunders, B. R.; Mears, S. J.; Cosgrove, T.; Vincent, B.; King, S. M.; Yu, G.-E. Poly(NIPAM) microgel particle de-swelling: a light scattering and small-angle neutron scattering study. *Colloids Surf., A* **1999**, *152*, 327−333.
(12) Sierra-Martín, B.; Romero-Cano, M. S.; Cosgrove, T.; Vincent, B.; Fernández-Barbero, A. Solvent relaxation of swelling PNIPAM microgels by NMR. *Colloids Surf., A* **2005**, *270−271*, 296−300.
(13) Hirotsu, S. Volume-phase transitions of ionized N-isopropylacrylamide gels. *J. Chem. Phys.* **1987**, *87*, 1392−1395.
(14) Hoare, T. R.; Pelton, R. Characterizing charge and crosslinker distributions in polyelectrolyte microgels. *Curr. Opin. Colloid Interface Sci.* **2008**, *13*, 413−428.
(15) Johansson, C.; Gernandt, J.; Bradley, M.; Vincent, B.; Hansson, P. Interaction between lysozyme and colloidal poly(NIPAM-co-acrylic acid) microgels. *J. Colloid Interface Sci.* **2010**, *347*, 241−251.
(16) Bradley, M.; Ramos, J.; Vincent, B. Equilibrium and Kietic Aspects of the Uptake of Poly(etylene oxide) by Copolymer Microgel Particles of N-Isopropylacrylamide and Acrylic Acid. *Langmuir* **2005**, *21*, 1209−1215.
(17) Smith, M. H.; Lyon, L. A. Tunable Encapsulation of Proteins within Charged Microgels. *Macromolecules* **2011**, *44*, 8154−8160.
(18) Horkay, F.; Hecht, A.; Grillo, I.; Basser, P. J.; Geissler, E. Experimental evidence for two thermodynamic length scales in neutralized polyacrylate gels. *J. Chem. Phys.* **2002**, *117*, 9103−9106.
(19) Horkay, F.; Hecht, A.; Geissler, E. Similarities Between Polyelectrolyte Gels and Biopolymer Solutions. *J. Polym. Sci., Part B: Polym. Phys.* **2006**, *44*, 3679−3686.
(20) Denton, A. R. Counterion penetration and effective electrostatic interactions in solutions of polyelectrolyte stars and microgels. *Phys. Rev. E* **2003**, *67*, 011804.
(21) Gottwald, D.; Likos, C. N.; Kahl, G.; Loewen, H. Ionic micro gels a model systems for colloids with an ultrasoft electrostatic repulsion: Structure and thermodynamics. *J. Chem. Phys.* **2005**, *122*, 074903.
(22) Hoare, T.; Pelton, R. Functionalized Microgel Swelling: Comparing Theory and Experiment. *J. Phys. Chem. B* **2007**, *111*, 11895−11906.
(23) Mohanty, P. S.; Richtering, W. Structural Ordering and Phase Behavior of Charged Microgels. *J. Phys. Chem. B* **2008**, *112*, 14692−14697.
(24) Fernández-Nieves, A.; Fernández-Barbero, A.; Vincent, B.; de las Nieves, F. J. Charge Controlled Swelling of Microgel Particles. *Macromolecules* **2000**, *33*, 2114−2118.
(25) Capriles-González, D.; Sierra-Martín, B.; Fernández-Nieves, A.; Fernández-Barbero, A. Coupled Deswelling of Multiresponsive Microgels. *J. Phys. Chem. B* **2008**, *112*, 12195−12200.
(26) Romeo, G.; Imperiali, L.; Kim, J.-W.; Fernández-Nieves, A.; Weitz, D. A. Origin of de-swelling and dynamics of dense ionic microgel suspensions. *J. Chem. Phys.* **2012**, *136*, 124905.
(27) Fernandez, P.; Schmidt, S.; Zeiser, M.; Fery, A.; Hellweg, T. Swelling and mechanical properties of polymer gels with cross-linking gradient. *Soft Matter* **2010**, *6*, 3455−3458.
(28) Lyon, L. A.; Debord, J. D.; Debord, S. B.; Jones, C. D.; McGrath, J. G.; Serpe, M. J. Microgel Colloidal Crystals. *J. Phys. Chem. B* **2004**, *108*, 19099−19106.
(29) Sorrell, C. D.; Lyon, L. A. Bimodal Swelling Responses in Microgel Thin Films. *J. Phys. Chem. B* **2007**, *111*, 4060−4066.
(30) Sorrell, C. D.; Lyon, L. A. Deformation Controlled Assembly of Binary Microgel Thin Films. *Langmuir* **2008**, *24*, 7216−7222.
(31) South, A. B.; Whitmire, R. E.; Garcia, A. J.; Lyon, L. A. Centrifugal Deposition of Microgels for the Rapid Assembly of Nonfouling Thin Films. *ACS Appl. Mater. Interfaces* **2009**, *1*, 2747−2754.
(32) Schmidt, S.; Zeiser, M.; Hellweg, T.; Duschl, C.; Fery, A.; Möhwald, H. Adhesion and Mechanical Properties of PNIPAM Microgel Films and their Potential Use as Switchable Cell Culture Substrates. *Adv. Funct. Mater.* **2010**, *20*, 3235−3243.
(33) Carter, M. C. D.; Sorrell, C. D.; Serpe, M. J. Deswelling Kinetics of Color Tunable Poly(N-Isopropylacrylamide) Microgel-Based Etalons. *J. Phys. Chem. B* **2011**, *115*, 14359−14368.
(34) Kim, J.; Serpe, M. J.; Lyon, L. A. Photoswitchable microlens arrays. *Angew. Chem., Int. Ed.* **2005**, *117*, 1357−1360.
(35) Kratz, K.; Hellweg, T.; Eimer, W. Influence of charge density on the swelling of colloidal poly(N-isopropylacrylamide-co-acrylic acid) microgels. *Colloids Surf., A* **2000**, *170*, 137−149.
(36) Snowden, M. J.; Chowdhry, B. Z.; Vincent, B.; Morris, G. E. Colloidal copolymer microgels of N-isopropylacrylamide and acrylic acid: pH, ionic strength and temperature effects. *J. Chem. Soc., Faraday Trans.* **1996**, *92*, 5013−5016.
(37) Burmistrova, A.; Richter, M.; Eisele, M.; Üzüm, C.; von Klitzing, R. The Effect of Co-Monomer Content on the Swelling/Shrinking and Mechanical Behaviour of Individually Adsorbed PNIPAM Microgel Particles. *Polymers* **2011**, *3*, 1575−1590.
(38) Nerapusri, V.; Keddie, J. L.; Vincent, B.; Bushnak, I. A. Swelling and Deswelling of Adsorbed Microgel Monolayers Triggered by Changes in Temperature, pH, and Electrolyte Concentration. *Langmuir* **2006**, *22*, 5036−5041.
(39) Höfl, S.; Zitzler, L.; Hellweg, T.; Herminghaus, S.; Mugele, F. Volume phase transition of ″smart″ micro gels in bulk solution and adsorbed at an interface: A combined AFM, dynamic light, and small angle neutron scattering study. *Polymer* **2007**, *48*, 245−254.
(40) Fernández-Barbero, A.; Fernández-Nieves, A.; Grillo, I.; López-Cabarcos, E. Structural modifications in the swelling of inhomogeneous microgels by light and neutron scattering. *Phys. Rev. E* **2002**, *66*, 051803.

(41) Berndt, I.; Pedersen, J. S.; Richtering, W. Temperature-Sensitive Core-Shell Microgel Particles with Dense Shell. *Angew. Chem., Int. Ed.* **2006**, *45*, 1737−1741.
(42) Ingo Berndt, P. L.; Jan Skov, Pedersen; Richtering, W. Influence of Shell Thickness and Cross-Link Density on the Structure of Temperature-Sensitive Poly-N-Isopropylacrylamide-Poly-N-Isopropylmethacrylamide Core-Shell Microgels Investigated by Small-Angle Neutron Scattering. *Langmuir* **2006**, *22*, 459−468.
(43) Stieger, M.; Richtering, W.; Pedersen, J. S.; Lindner, P. Small-angle neutron scattering study of structural changes in temperature sensitive microgel colloid. *J. Chem. Phys.* **2004**, *120*, 6197−6206.
(44) Müller-Buschbaum, P. Grazing incidence small-angle neutron scattering: challenges and possibilities. *Polym. J.* **2013**, *45*, 34−42.
(45) Müller-Buschbaum, P.; Gutmann, J. S.; Cubitt, R.; Stamm, M. Probing the in-plane composition of thin polymer films with grazing-incidence small angle scattering and atomic force microscopy. *Colloid Polym. Sci.* **1999**, *277*, 1193.
(46) Müller-Buschbaum, P.; Gutmann, J. S.; Stamm, M.; Cubitt, R. Surface structure analysis of thin dewetted polymer blend films. *Macromol. Symp.* **2000**, *149*, 283.
(47) Pelton, R. Temperature-sensitive aqueous microgels. *Adv. Colloid Interface Sci.* **2000**, *85*, 1−33.
(48) Hoare, T. R.; Kohane, D. S. Hydrogels in drug delivery: Progress and challenges. *Polymer* **2008**, *49*, 1993−2007.
(49) Rabin, Y.; Panyukov, S. Scattering profiles of Charged Gels: Frozen Inhomogeneities, Thermal Fluctuations, and Microphase Separation. *Macromolecules* **1997**, *30*, 301−312.
(50) Ikkai, F.; Suzuki, T.; Karino, T.; Shibayama, M. Microstructure of N-Isopropylacrylamide-Acrylic Acid Copolymer Gels Having Different Spatial Configurations of Weakly Charged Groups. *Macromolecules* **2007**, *40*, 1140−1146.
(51) Korolkov, D.; Busch, P.; Willner, L.; Kentzinger, E.; Rücker, U.; Paul, A.; Frielinghaus, H.; Brückel, T. Analysis of randomly oriented structures by grazing-incidence small-angle neutron scattering. *J. Appl. Crystallogr.* **2012**, *45*, 245−254.
(52) Salditt, T.; Metzger, T. H.; Peisl, J.; Reinker, B.; Moske, M.; Samwer, K. Determination of the height-height correlation function of rough surfaces from diffuse X-ray scattering. *Europhys. Lett.* **1995**, *32*, 331.
(53) Matzelle, T. R.; Geuskens, G.; Kruse, N. Elastic Properties of Poly(N-isopropylacrylamide) and Poly(acrylamide) Hydrogels Studied by Scanning Force Microscopy. *Macromolecules* **2003**, *36*, 2926−2931.
(54) Kratz, K.; Hellweg, T.; Eimer, W. Structural changes in PNIPAM microgel particles as seen by SANS, DLS, and EM techniques. *Polymer* **2001**, *42*, 6531−6539.
(55) Schemmel, S.; Akcakayiran, D.; Rother, G.; Brulet, A.; Farago, B.; Hellweg, T.; Findenegg, G. H. Phase Separation of a Binary Liquid System in Controlled-Pore Glass. *Mater. Res. Soc. Symp. Proc.* **2004**, *790*, P.7.2.1−P.7.2.6.
(56) Formisano, F.; Teixeira, J. Critical fluctuations of a binary fluid mixture confined in a porous medium. *Eur. Phys. J. E* **2000**, *1*, 1−4.
(57) Konieczny, M.; Likos, C. N. Polyelectrolyte stars in planar confinement. *J. Chem. Phys.* **2006**, *124*, 214904−1−214904−12.
(58) Karg, M.; Prévost, S.; Brandt, A.; Wallacher, D.; von Klitzing, R.; Hellweg, T. In *Intelligent Hydrogels*; Sadowski, G., Richtering, W., Eds.; Progress in Colloid and Polymer Science; Springer: Cham, 2013; Vol. *140*; pp 63−76.
(59) Burmistrova, A.; von Klitzing, R. Control of number density and swelling/shrinking behavior of P(NIPAM-AAc) particles at solid surfaces. *J. Mater. Chem.* **2010**, *20*, 3502−3507.